Introduction to fNIRS Imaging - William Meng

Team Members: William Meng

December 17, 2022

Introduction

Functional Near Infrared Spectroscopy (fNIRS) is a non-invasive and safe brain imaging modality which uses changes in the absorption of Near Infrared Light (NIR) to estimate changes in blood oxygen saturation, which is a proxy for brain activity. Compared to fMRI, fNIRS is much less expensive and allows the patient to move freely.

Conventional optical imaging techniques rely on the spatial mapping of the scene radiance onto an image plane, provided by a pinhole or lens, in order to produce an image of the scene. This mapping is not valid in the case of brain imaging because light is scattered many times as it propagates through biological tissue. Therefore, one cannot simply point a camera at the brain and measure the radiance within the brain with any meaningful spatial resolution.

fNIRS takes a different approach: an array of light sources and detectors are arranged such that each source/detector pair constitutes a "channel" in which light flows from source to detector through a designated tissue region. By measuring the amount of light which flows through the channel, one can estimate the bulk optical properties within the tissue region of the channel. From the bulk optical properties measured at multiple wavelengths, one can then estimate the concentration of different chromophores such as oxygenated hemoglobin (HbO2) and deoxygenated hemoglobin (Hb), which serve as indicators for local neural activity.

In this project, we focus on Continuous Wave (CW) fNIRS, which measures the (quasi) steady state optical properties of each channel. Other types of fNIRS include Time Domain (TD) and Frequency Domain (FD) fNIRS, which measure Time of Flight (ToF) information in order to separate the channel into multiple depth planes.

Background

Channel Geometry

The standard geometry for a single fNIRS channel has the source and detector placed at the surface of the tissue, separated by a distance which is known as the source/detector (S/D) distance.

Light flows from the source to the detector through a channel which is roughly shaped like a banana. Note that light is not strictly confined within any particular region with a sharp boundary, rather the illustration of the channel in Fig. 1a represents the region where photons will travel with greatest probability, and the probability falls off gradually as one moves away from it. A shorter S/D distance results in a shallower channel, whereas a longer S/D distance results in a deeper channel. A S/D distance of 30 mm is typically used to yield a channel at the relevant depth for brain imaging.

The source is typically an LED or a laser, which can either be placed in direct contact with the tissue or coupled through a fiber. The detector is typically an Avalanche Photodiode (APD), which has much higher sensitivity than a conventional photodiode. This additional detector sensitivity is needed to overcome the large attenuation of light due to absorption and scattering while keeping the source power within reasonable limits for safety and practical reasons.

In order to perform multispectral measurements for each channel, multiple sources of different wavelengths are placed in close proximity such that they can be considered to originate from the same source location. These sources are typically time multiplexed so that a single detector can be used for multispectral measurements, rather than using multiple detectors with a color filter array.

In order to image the whole brain, multiple sources and detector are arranged such that the channels cover areas of interest in the brain.

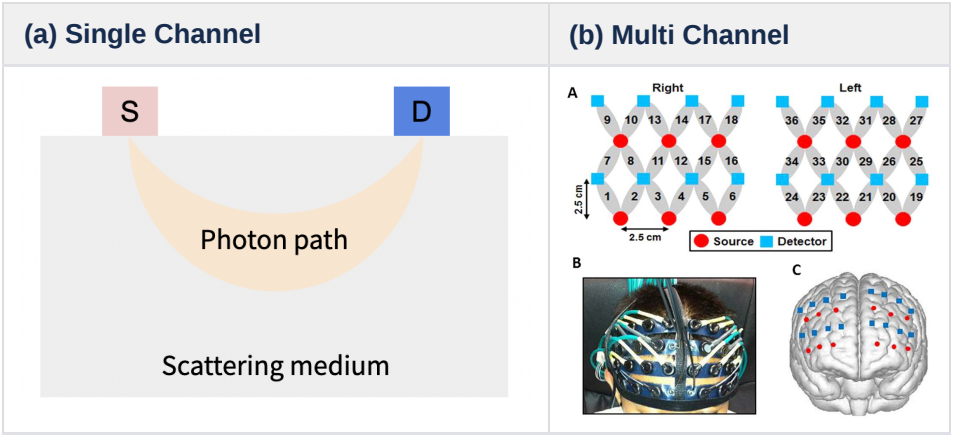

Figure 1: (a) Side view of a single channel. (b) Overhead view of multiple channels, reproduced from Yennu et al (2014).

Hemoglobin Absorption Spectra

Neural activity causes local changes in blood oxygen level, which can be quantified via changes in HbO2 and Hb concentrations. An increase in blood oxygen saturation is marked by an increase in HbO2 concentration and decrease in Hb concentration, whereas a decrease in blood oxygen saturation is marked by an increase in Hb concentration and decrease in HbO2 concentration. In the NIR window (roughly 700-900nm), the absorption coefficient of HbO2 is roughly an increasing function of wavelength, and the absorption coefficient of Hb is roughly a decreasing function of wavelength. Therefore, the absorption coefficients at a short and a long wavelength within this window (eg. 700nm and 900nm) constitute a differential signal pair which is strongly correlated with the blood oxygen level and is robust to common-mode changes (ie. changes in absorption for extraneous reasons which affect both long and short wavelengths). Therefore, if one can measure the absorption coefficients at two wavelengths at opposite ends of the NIR window, one can estimate blood oxygen saturation.

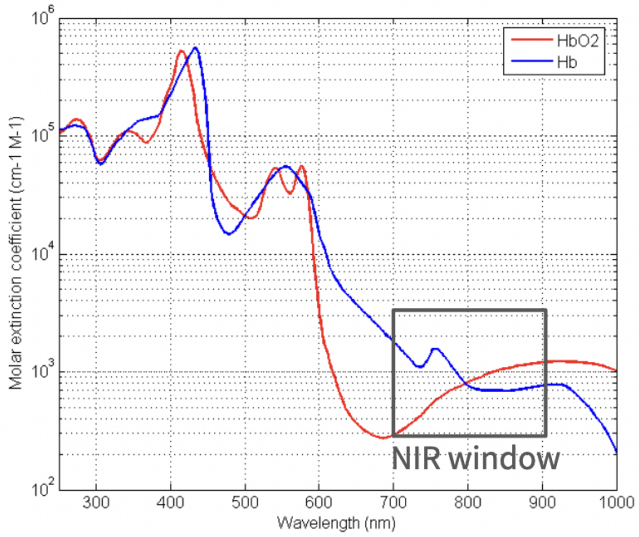

Figure 2: Absorption spectra of HbO2 and Hb. Original image from Wikipedia.

Beer Lambert Law (BLL)

The fundamental principle which allows one to estimate the concentration of a chromophore from a measurement of the light attenuated by a channel is the Beer Lambert Law. In the ideal slab geometry (where the source and detector are on opposing sides of the slab such that light travels in a straight line), the Beer Lambert Law is given by:

$$A = \varepsilon \ell \chi$$

where A is absorbance, ε is the molar extinction coefficient of the chromophore, ℓ is the path length, and χ is the concentration of the chromophore.

It is often more convenient to work in terms of the absorption per unit length:

$$\mu_a = 2.303 \varepsilon \chi / 645000$$

where μ_a is the absorption coefficient in 1/mm.

Assuming a hemoglobin concentration of 150 g/L in blood, this becomes

$$\mu_a = 0.00054 \varepsilon$$

In a typical fNIRS configuration, the Beer Lambert Law takes a somewhat more complicated form due to the use of multiple wavelengths and the unknown path length.

Results

Simplified Multilayer Brain Model

We consider a simplified 2D multilayer model of the brain's optical properties, using typical values from the literature.

Figure 3: A simplified multilayer model representing the optical properties of various layers found in the human brain.

Layer	Thickness (mm)	Absorption Coefficient μ_a (1/mm)	Scattering Coefficient μ_s (1/mm)
Scalp	2	0.017275	0.72
Skull	8	0.011925	0.92
Cerebral Spinal Fluid (CSF)	5	0.002500	0.01
Gray matter	15	0.019500	1.10
White matter	20	0.016900	1.35

For simplicity, we assume that the scattering anisotropy is g=0.9 and the index of refraction is n=1.4 everywhere.

In particular, note that the Cerebral Spinal Fluid (CSF) layer has very low absorption and scattering compared to the other layers. Therefore, we should expect photon transport through the CSF to be nearly ballistic.

Monte Carlo Simulation Parameters

The spatial distribution of photons in a scattering medium is described by the Radiative Transfer Equation, however this cannot be solved analytically except in extremely simple geometries (eg. infinite homogeneous slab). Instead, a numerical approach via Monte Carlo simulation can be used for more practical scenarios. This involves launching many photons and tracing out possible paths for them, according to the given scattering and absorption coefficients throughout the medium. If a very large number of photons is simulated, the sampled paths will closely approximate the true probability distribution for the photon paths.

The Monte Carlo eXtreme (MCX) software was used in this project to simulate photon propagation in the simplified multilayer brain model, using the following parameters:

- *Source Beamwidth:* 60º
- *Detector Acceptance Angle:* 60º
- *Short Channel Spacing:* 5mm
- *Long Channel Spacing:* 30mm
- *Integration Time:* 10 ns
- *Number of Photons Launched:* 1e7

Photon Path Spatial Distributions

The spatial distribution of photons in the simplified multilayer brain model was quantified with Monte Carlo simulations. Fig. 4a shows the density of photon paths originating from the source and propagating throughout the volume. Fig. 5b and Fig. 5c show the density of photon paths originating from the source and reaching the detector for the short and long channels, respectively. The short channel is mostly confined to shallow regions including the scalp and skull, whereas the long channel penetrates deeper and includes the gray matter region, which is of prime interest for functional brain imaging.

(a) Source → Volume	(b) Source → Volume → Detector (Short Channel)	(c) Source → Volume → Detector (Long Channel)
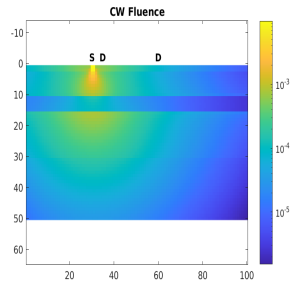	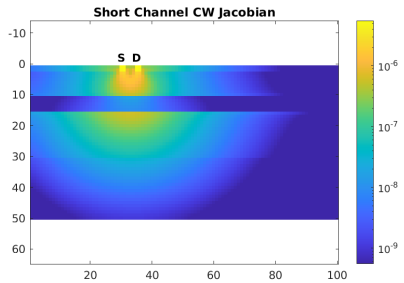	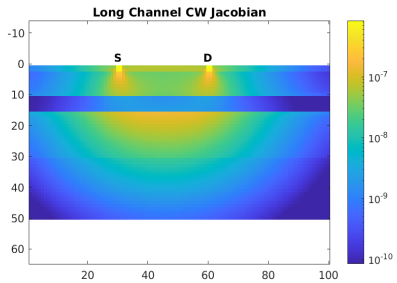

Figure 4: (a) The spatial distribution for photon paths originating from the source, (b) originating from the source and arriving at the short channel detector 5 mm away from the source, and (c) originating from the source and arriving at the long channel detector 30 mm away from the source. All values are given in Joules and normalized to a source energy of 1 Joule.

There is a discontinuity in the density of paths along the boundaries of the CSF region, with a much lower density of paths within the CSF region. While such a discontinuity would be impossible when light propagates without scattering, it is a perfectly reasonable result for inhomogeneous scattering media. Light is scattered many times as it propagates in the regions above and below the CSF (which have a high scattering coefficient), but it is nearly ballistic (ie. traveling straight through without scattering) in the CSF (which has a low scattering coefficient). Therefore, the density of paths is lower in the CSF, even when every photon in the region below had to travel through the CSF to get there. As a simple analogy, imagine the many photon paths being traced out by a pencil. A region with high scattering will appear

much darker since the pencil will scribble over it many times, whereas a region with low scattering will appear lighter as the pencil passes through it with only a few traces.

Channel Sensitivity

First, we consider the sensitivity of the long channel (with a source/detector distance of 30mm) to the absorption coefficient in the gray matter layer. This result is agnostic to wavelength, since the absorption coefficient for each wavelength is determined by the absorption spectra and concentrations of the chromophores present. For simplicity, we assume there are no changes in absorption in regions other than the gray matter layer.

Instead of intensity, it is typically more convenient to work in terms of Optical Density, which measures how much the incident light is attenuated by propagation through the medium on a logarithmic scale:

$$\mathrm{OD} = \log_{10}\left(\frac{I_{\text{incident}}}{I_{\text{transmitted}}}\right)$$

In Fig. 5a, we see that the long channel's optical density is a nonlinear function of the absorption coefficient in the gray matter layer. However, if we consider only a small change in μ_a, such as that due to changes in blood oxygen level, we can consider the relationship to be approximately linear.

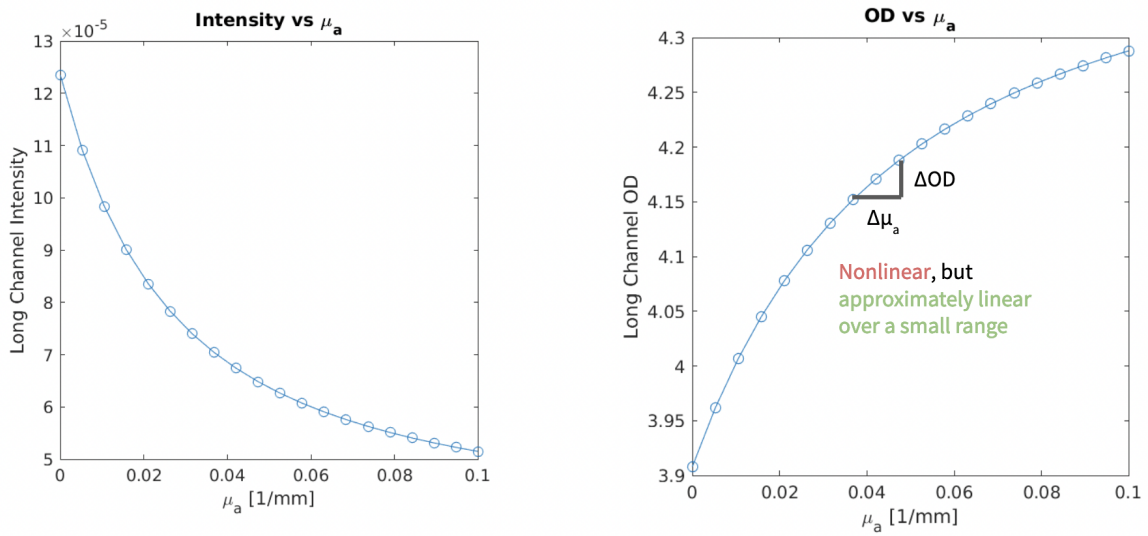

Figure 5: (a) Intensity measured at the long channel detector as a function of μ_a in the gray matter layer. (b) Optical density of the long channel as a function of μ_a in the gray matter layer.

Next, we compute the absorption coefficient at various wavelengths as a function of blood oxygen saturation, and then plot optical density as a function of wavelength for various levels of blood oxygen saturation. For simplicity, we assume that the cerebral blood volume and concentration of total hemoglobin is constant in the region of interest, such that the changes in HbO2 and Hb are equal and opposite. Using 150g/L as the concentration of hemoglobin in blood and 3.5% as the volumetric proportion of blood in gray matter, we can express the absorption coefficients at each wavelength as:

$$\mu_{a_\lambda} = 0.019500 + 0.035 \times 0.00054(\varepsilon_{\lambda,\mathrm{Hb}} + \varepsilon_{\lambda,\mathrm{HbO2}})$$

The molar extinction coefficients for HbO2 and Hb at each wavelength can be found in the tabulated data compiled by Scott Prahl. The wavelengths chosen for this simulation data shown in Fig. 6 were 775, 810, 870, and 904 nm, in accordance with the popular UCL4 formula for fNIRS systems. Note that the molar extinction coefficients for 775 nm are interpolated from the neighboring values for 774 and 776 nm.

Wavelength (nm)	775	810	870	904
$\varepsilon_{\lambda,\mathrm{HbO2}}$	683.2	864	1128	1206
$\varepsilon_{\lambda,\mathrm{Hb}}$	1188.28	717.08	705.84	767.44

Using these values, we can again run Monte Carlo simulations to find the optical density at each wavelength for various levels of blood oxygen saturation, as shown in Fig. 6.

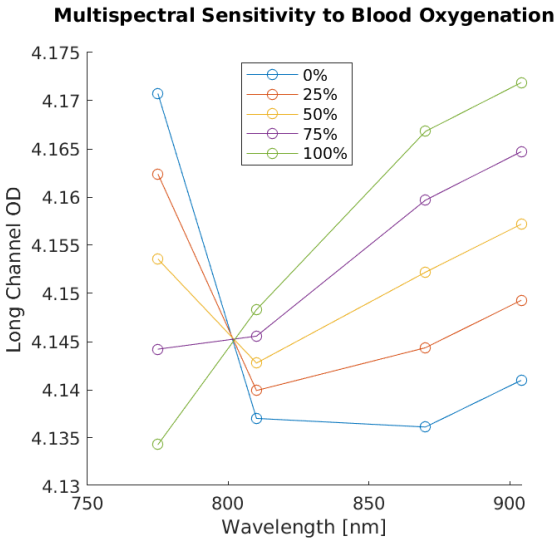

Figure 6: Optical density of the long channel as a function of wavelength for various levels of blood oxygen saturation.

Chromophore Estimation

Finally, we can estimate the changes in HbO2 and Hb concentrations from multispectral measurements of the optical density of the long channel. The UCL4 algorithm is a popular formula for performing this estimation:

$$\begin{pmatrix} \Delta \mathrm{Hb} \\ \Delta \mathrm{HbO_2} \\ \Delta \mathrm{Cyt} \end{pmatrix} = \begin{pmatrix} 1.58 & -1.35 & -0.57 & 0.68 \\ -0.66 & -0.85 & 0.56 & 1.5 \\ -0.26 & 1.17 & 0.12 & -0.92 \end{pmatrix} \begin{pmatrix} \Delta \mathrm{OD}_{775\ \mathrm{nm}} \\ \Delta \mathrm{OD}_{810\ \mathrm{nm}} \\ \Delta \mathrm{OD}_{87\ \mathrm{mm}} \\ \Delta \mathrm{OD}_{904\ \mathrm{nm}} \end{pmatrix}$$

The matrix shown above can be derived from the pseudo-inverse of the matrix of molar extinction coefficients for each wavelength of interest. We ignore the term for changes in cytochrome oxidase ($\Delta \mathrm{Cyt}$) as we are only considering HbO2 and Hb.

Using 50% blood oxygen saturation as the reference level, we estimated the changes in HbO2 and Hb while sweeping blood oxygen saturation from 0 to 1. As shown in Fig. 6, HbO2 concentration increases monotonically and Hb concentration decreases monotonically, as expected.

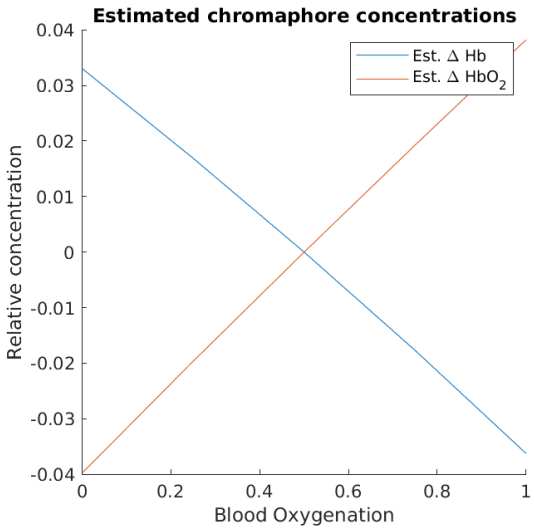

Figure 7: Estimated chromophore concentrations as a function of blood oxygen saturation, under the assumption of constant cerebral blood volume and total hemoglobin concentration in the region of interest.

In reality, the changes in HbO2 and Hb concentrations would not be equal and opposite. In a real brain, additional oxygen rich blood is pumped into regions with neural activity, temporarily creating a surplus of HbO2 beyond that which is needed to replace the existing Hb. As a result, the changes in HbO2 concentration tend to be larger than the corresponding changes in Hb concentration, as shown in Fig. 3 of Pinti et al.

Conclusion

In conclusion, we performed simulations of a typical CW fNIRS imaging system with a simplified 2D multilayer model of the human brain. Using standard values for cerebral blood value and hemoglobin concentration along with the absorption spectra of oxygenated hemoglobin (HbO2) and deoxygenated hemoglobin (Hb), we simulated the optical density at 4 different NIR wavelengths with a source/detector spacing of 30 mm. We then estimated the changes in HbO2 and Hb concentrations using the UCL4 algorithm.

Appendix

Time Gated fNIRS

Photons traveling along paths at shallow depths tend to have a shorter time of flight than photons traveling along paths at deeper depths. Therefore, a pulsed illumination source combined with a time-gated detector can be used to reject photons traveling at shallower depths, thus improving the depth selectivity of the channel.

Diffuse Optical Tomography (DOT)

Using a denser array of sources and detectors in conjunction with Time of Flight (ToF) measurements, it is possible to reconstruct the 3D profile of absorption with greater spatial resolution than a bulk parameter estimation. State of the art Diffuse Optical Tomography (DOT) techniques can reconstruct images with mm-scale resolution. However, these techniques typically cannot be run in real time because they require solving an ill-posed inverse problem, which is typically done via an iterative approach with a computationally expensive forward model.

References

Naseer N and Hong K-S (2015) fNIRS-based brain-computer interfaces: a review. *Front. Hum. Neurosci.* **9**:3

A. Yennu, F. Tian, A. Smith-Osborne, and H. Liu, "Investigation of Prefrontal Hemodynamics of PTSD Patients While Performing Stroop Task Using fNIRS," in *Biomedical Optics 2014*, OSA Technical Digest (online) (Optica Publishing Group, 2014), paper BW2B.7.

Qianqian Fang and David A. Boas, "Monte Carlo Simulation of Photon Migration in 3D Turbid Media Accelerated by Graphics Processing Units," Opt. Express **17**, 20178-20190 (2009)

Scott Prahl, "Optical Absorption of Hemoglobin," omlc.org.

S.J. Matcher, C.E. Elwell, C.E. Cooper, M. Cope, D.T. Delpy, "Performance Comparison of Several Published Tissue Near-Infrared Spectroscopy Algorithms," Analytical Biochemistry, Volume 227, Issue 1, 1995, Pages 54-68.

Pinti, P., Tachtsidis, I., Hamilton, A., Hirsch, J., Aichelburg, C., Gilbert, S. and Burgess, P.W. (2020), The present and future use of functional near-infrared spectroscopy (fNIRS) for cognitive neuroscience. Ann. N.Y. Acad. Sci., 1464: 5-29.

Hyun Keol Kim, Yongyi Zhao, Ankit Raghuram, Ashok Veeraraghavan, Jacob Robinson, Andreas H. Hielscher, "Ultrafast and Ultrahigh-Resolution Diffuse Optical Tomography for Brain Imaging with Sensitivity Equation based Noniterative Sparse Optical Reconstruction (SENSOR)," Journal of Quantitative Spectroscopy and Radiative Transfer, Volume 276, 2021.

Code

To run the above code, you need an Nvidia GPU with CUDA support. I have only tested this code on 64 bit Linux, but other platforms may work as well.

You then need to install the MCXLab library for Matlab:

- Follow the instructions here to install the MCX software package which includes MCXLab, or...
- ...for convenience, I've uploaded a ZIP file below of just the MCXLab folder in case you don't want to install the entire MCX software. Simply extract the ZIP and add the resulting folder to your Matlab path.

Slides


Introduction to
fNIRS Imaging
William Meng
wlmeng@stanford.edu
PSYCH 221
December 14, 2022
PDF